Origin of the Mode Splitting Effect in a Microwave Sapphire Whispering Gallery Mode Resonator

Vincent Giordano, Samuel Margueron

Abstract—Cylindrical Whispering gallery modes (WGM) resonators, machined from high-quality sapphire mono-crystal and cooled to liquid helium temperature, exhibit exceptionally high Q-factors in the microwave frequency domain. Such resonators serve as the core for ultra-stable oscillator featuring fractional frequency stability exceeding 1×10^{-15} at short integration times. Similar to any cylindrical resonant structure, the WGM resonator exhibits a two-fold degeneracy. When a defect disrupts the cylindrical symmetry of the resonator, the WGMs split and appear as doublets. In the high-quality sapphire resonators, the frequency separation between these twin modes varies from one mode order to another, reaching a maximum value of a few tens of kHz. While mode splitting for a given mode was previously deemed unpredictable and intrinsic to each resonator, assumed to result from randomly distributed defects, our findings indicate that the observed mode splitting in all sapphire resonators, regardless of their origin, primarily arises from a common defect due to the different response of the sapphire's crystallographic plans to the manufacturing processes.

Index Terms—Mode degeneracy, sapphire crystal, ultra-stable oscillator, whispering gallery mode resonator.

I. INTRODUCTION

Whispering gallery modes low loss dielectric resonators have found widespread applications in the fields of microwaves, millimeter waves and optics. The strong confinement of the electromagnetic field within the dielectric medium achieved through these excitation modes, imparts exceptional properties to the resonator such as: high quality factor (when associated with low loss dielectric as sapphire), immunity to environment perturbations, enlarged dimensions compared with classical $TE_{01\delta}$ mode (advantageous for mm-wave or photonics components). In the microwave domain, these resonators serve as frequency reference to achieve ultra-stable cryogenic oscillators [1], [2], [3], [4], and facilitate accurate measurements of material complex permittivity [5] or the surface impedance of superconductors [6]. Planar WGM dielectric resonators have been employed in the development of millimeter-wave filters, oscillators, and multiple-port power dividers/combiners [7], [8]. While it is certainly in the field of photonics that we find today the most innovative applications of WGMs with a profusion of resonator shapes, sizes and operating wavelengths [9], [10].

A wide variety of resonator shapes such as disks, rings, toroids or spheres, can sustain the propagation of WGMs. The rotational symmetry of these resonators leads to a degeneration of the solutions of the Helmholtz equation, yielding the two-fold degeneracy of the WGMs. Any deviation from the resonator's symmetry, induced by a defect, lifts this degeneracy, and a resonance line splitting is generally observed [11], [12]. Such defects can manifest as a geometrical imperfections, particles adhering to the resonator surface or inhomogeneities within the dielectric bulk [13], [14]. For many applications, this phenomenon proves detrimental. In the case of a microwave WGM resonator oscillator, frequency jumps between the two degenerate modes can compromise the oscillator stability [15], [16], [17]. Conversely, in photonics WGM resonators, the degeneracy and line splitting phenomenon can be harnessed for sensing nanoparticles, such as contaminants or viruses [18], [19]. Regardless of the application, enhanced control over mode splitting and a deeper understanding of its origin would be beneficial.

Until now, the prevailing guess attributes the mode splitting observed in sapphire microwave WGM resonators to randomly situated defects affecting the resonator's geometry or homogeneity. Contrary to this widespread belief, our paper challenges this idea and demonstrates that mode splitting originates from a precisely determined geometrical defect. This defect is consistently observed in all sapphire resonators, irrespective of their origin. Notably, it aligns with the 6-fold symmetry of the sapphire crystal and correlates with the distinct crystallographic planes, which respond differentially during the sapphire machining process.

As a secondary outcome of our study, we offer here a modest answer to the question *Can One Hear the Shape of a Drum?* posed by M. Kac in 1966 in his renowned article [20]. It took mathematicians approximately thirty years to provide a general negative answer to this question [21]. It is also noteworthy that the first experimental verification of the isospectrality of two distinct geometries, as discovered by mathematicians was carried out using hollow metal microwave cavities as a drum [22]. While we do not delve into the intricacies of this complex mathematical problem in this article, we show how the phenomenon of mode-splitting

V. Giordano, S. Margueron are with the Institute FEMTO-ST (Franche-Comté Electronique, Mécanique, Thermique et Optique - Sciences et Technologies), CNRS (Centre National de la Recherche Scientifique), Supmicrotech-ENSMM (Ecole Nationale Supérieure de Mécanique et des Microtechniques), Université de Franche-Comté, 25000 Besançon France, (e-mail: giordano@femto-st.fr)

observed in a microwave whispering gallery mode sapphire resonator allows for the deduction of its deviation from the ideal cylindrical form.

II. THE CRYOGENIC SAPPHIRE RESONATOR

The mono-crystal of Al_2O_3, or sapphire, stands out as the material with the lowest dielectric losses in the microwave frequency range. With a loss tangent ($\tan\delta$) of approximately 5×10^{-6} at 300 K and lower than 10^{-9} at liquid helium temperature [23], it is an ideal dielectric for constructing high Q-factor microwave resonators in X-band. Despite its low relative permittivity ($\epsilon_r \approx 10$), sapphire's high azimuthal order modes, known as whispering gallery modes, are strategically utilized to fully exploit its low dielectric loss tangent. A standard design consists of a large sapphire disk, typically 30 to 50 mm in diameter (for X-band operation), housed within a metallic cylindrical cavity. In the case of a whispering-gallery mode, total reflection occurs at the curved air–dielectric interface, effectively limiting the power dissipation in the metallic enclosure walls. Consequently, the resonator's unloaded Q-factor (Q_0) is only limited by the sapphire dielectric losses:

$$Q_0 \approx \frac{1}{\tan\delta} \quad (1)$$

Since 2010, we have successfully constructed and validated a dozen of ultra-stable Cryogenic Sapphire Oscillators (CSO) at the FEMTO-ST Institute, all based on this cutting-edge technology. Our most advanced design is currently available as a commercial instrument under the codename: ULISS-2G [24], [25], [26]. Describing the (in)stability as the Allan deviation (ADEV) $\sigma_y(\tau)$ of the fractional frequency y as a function of the measurement time τ, ULISS-2G features $\sigma_y(\tau) < 3 \times 10^{-15}$ for $1 \text{ s} \leq \tau \leq 10^4 \text{ s}$ and is limited by a drift of $\approx 10^{-14}$ at one day. It can run unattended for years of continuous operation, requiring only simple maintenance every 2nd year.

All the resonators incorporated into our CSOs are manufactured according to the same design, as illustrated in Fig. 1 [27].
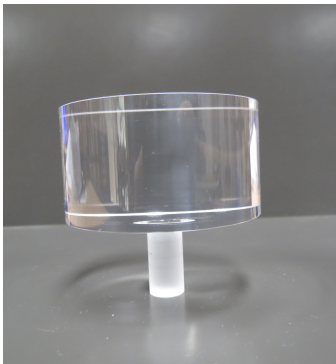
Fig. 1. *ULISS-2G sapphire resonator.*

Made in a high purity sapphire mono-crystal, it is 54 mm in diameter and 30 mm in height, with the cylindrical axis parallel to the Al_2O_3 crystal c-axis within $1°$. The 10 mm diameter spindle machined from the bulk is used to attach the resonator to the bottom flange of a gold plated standard Oxygen-free high-thermal-conductivity (OFHC) copper cavity. This copper cavity has an internal diameter of 85 mm. The resonator operates on the quasi-transverse magnetic whispering-gallery mode $WGH_{15,0,0}$ resonating at $\nu_{15} = 9.99$ GHz [28]. Two diametrically opposed small magnetic loops constitute the input and output resonator ports. These magnetic probes are formed from the internal conductor of a copper UT085 coaxial cable. The loop area is $\approx 1.5 \text{ mm}^2$. The radial position of these probes can be adjusted to tune the coupling coefficient at each resonator port. In practice and for the operating mode, the resonator is nearly critically coupled at its input port and weakly coupled at its output: $\beta_1 \sim 1$ and $\beta_2 \leq 0.01$. To achieve critical coupling, the input coupling probe penetrates a few millimeters into the cavity. In that conditions, the resonator coupling induces a very weak perturbation to the resonator frequency. Indeed, the fractional frequency shift induced by the input port coupling is [29]:

$$\frac{\Delta\nu}{\nu} = -\frac{\beta_1}{2Q_0}\frac{X_G}{Z_0} \quad (2)$$

where $Z_0 = 50 \ \Omega$ the line impedance and X_G is the impedance reactive part of the circuit connected to the resonator input port, in the worst experimental conditions $X_G < 5 \ \Omega$. Due to the high unloaded Q-factor, the induced fractional frequency shift is always less than 1×10^{-10}, and thus completely negligible with respect to the other causes of perturbation. In the following calculations, the impact of the coupling probes are neglected. The cavity is thermally linked to the 2nd-stage of a Pulse-Tube cryocooler and stabilized near 6 K.

III. THE MODE DEGENERACY

Although WGM are strictly hybrid modes, they can be classified in quasi-TM (WGH) and quasi-TE (WGE) mode families. A WGH mode is characterized by the electric field mainly directed in the axial direction while its magnetic field is essentially transverse. Conversely, for a WGE mode, the situation is inverted. Whispering gallery modes can be further characterized by three integers, i.e. m, n and l, representing the variation of the electromagnetic field components in the azimuthal (ϕ), radial (r) and axial (z) directions of the cylindrical coordinate frame. In our developments, we specifically focus on the $WGH_{m,0,0}$ modes, which exhibit the highest Q-factor. For these modes, the axial electric field inside the sapphire can be expressed as [30]:

$$E_z(r,\phi,z) = E_m J_m(kr)\cos(\beta z)\begin{cases}\cos(m\phi)\\\sin(m\phi)\end{cases} \quad (3)$$

where E_m is the electric field amplitude, J_m is the Bessel function of the first kind of order m, β denotes the axial propagation constant and k is the guided wave number. The brace indicates that the resonator can support two orthogonal modes, both equivalent solutions of the Helmholtz equation.

In a perfect sapphire cylinder, the twin modes probe exactly the same medium, and thus resonate at the same frequency. The position of the nodes of the stationary wave pattern is set by the coupling structure. Previous studies have demonstrated how any defect that affects the resonator cylindrical symmetry lifts the degeneracy of the twin modes [11]. The frequency splitting, denoted $\delta\nu_m$, between the twin modes is dependent on the azimuthal number m, as m conditions the electromagnetic field configuration within the sapphire crystal. For example, the impact of a localized defect affecting the dielectric properties of the medium, will be higher for modes exhibiting a maximum of the electric field near the defect position. It is worth noting that in presence of the defect, the azimuthal position of the stationary wave pattern is no longer set by the coupling structure, but remains locked to the defect. One of the twin mode has a node at the defect location, the second one has a maximum.

In the CSO we exploit the mode $WGH_{15,0,0}$ at $\nu_{15} = 9.99$ GHz for which the twin resonances have always been observed. $\delta\nu_{15}$ typically falls within the order of 10 kHz (10^{-6} in relative value). Fig. 2 shows the two $WGH_{15,0,0}$ modes of a typical sapphire resonator as experimentally observed with a Vector Network Analyzer after a first cooling near 6 K. Here, the calibration planes are set at the level of the cryostat RF feedthroughs. Thus, the cryogenic cables linking the resonator to the cryostat external flange are part of the measured assembly. For this particular sapphire resonator, we have $\delta\nu_{15} = 8.6$ kHz ($\frac{\delta\nu_{15}}{\nu_{15}} \approx 0.9 \times 10^{-6}$). In this particular case, the insertion losses of the two modes are nearly the same, which can lead to frequency instability for the oscillator.
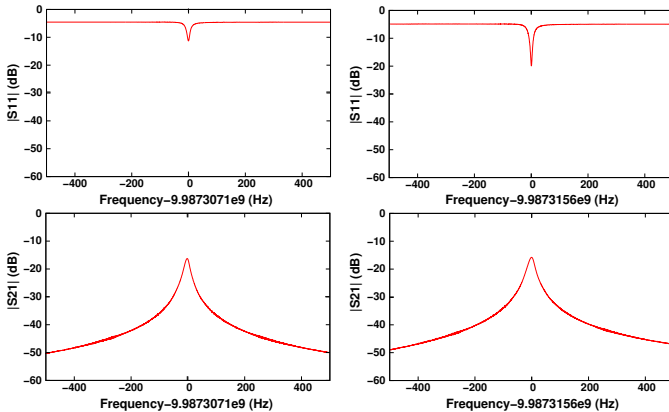
Fig. 2. $|S_{11}|$ and $|S_{21}|$: magnitude of the reflection and transmission coefficients for the twin modes $WGH_{15,0,0}$ observed during the first cooling down to 6 K.

The presence of the twin modes poses a challenge for our application. Indeed, the oscillator will start on the mode with the lower insertion losses (higher coupling). The latter will be hardly predictable before cooling as the degeneracy lifting is not observable at room temperature. In unfavorable scenarios, both modes may exhibit equivalent insertion losses, potentially jeopardizing the oscillator stability due to random frequency jumps. This issue has been solved by rotating the sapphire resonator with respect to the coupling probes position,

effectively suppressing the mode with the lowest frequency, as demonstrated in Fig. 3.
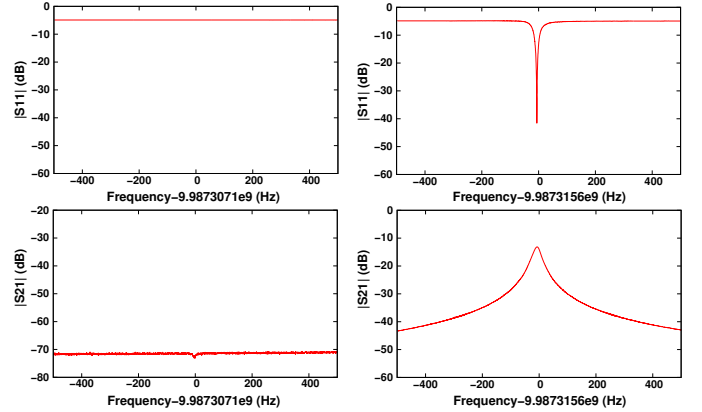
Fig. 3. $|S_{11}|$ and $|S_{21}|$: magnitude of the reflection and transmission coefficients for the twin modes $WGH_{15,0,0}$ measured after a resonator rotation and a second cooling down to 6 K. The sapphire rotation favoured the higher frequency mode, which is now the only mode that can oscillate.

Apart the $WGH_{15,0,0}$ mode, which serves as frequency reference for our oscillator, the experimental setup allows for the observation of other WGH modes spanning from approximately 4 GHz to 14 GHz corresponding to $5 \leq m \leq 24$. Beyond this range, the constrained bandwidth of the isolators positioned at each resonator port and the poor coupling of the remaining modes typically render their detection impractical.

Until now, we had not extensively investigated the origin of mode splitting. As the disturbances leading to the mode splitting should be randomly distributed, the various $\delta\nu_m$ are challenging to predict and were believed to be specific to each resonator. In our opinion, this assertion must be reconsidered, as demonstrated in Fig. 4.
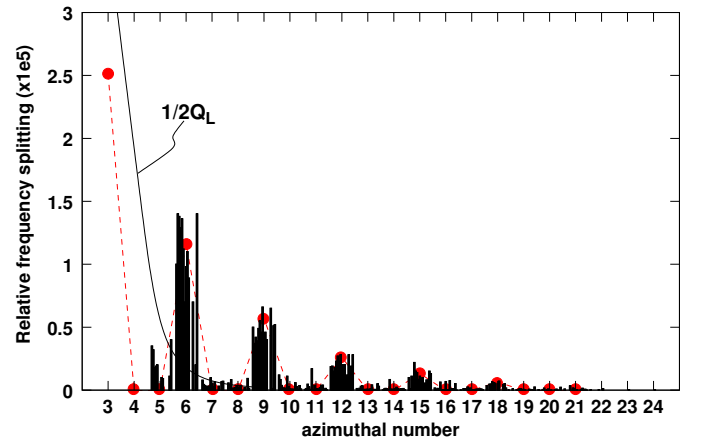
Fig. 4. Compilation of the relative mode splitting $\delta\nu_m/\nu_m$. For a given azimuthal number m, each resonator is represented by a black bar. The red bullets represent the calculation result obtained with $\Delta r = 1.3$ μm (see section IV).

Fig. 4 compiles the relatives values of $\delta\nu_m/\nu_m$ measured across more than fifteen resonators sourced from various manufacturers, each overseeing the entire processing chain from crystal growth to final polishing. Some of these resonators have been ordered more than ten years ago. The tested resonators come from three different manufacturers located on distinct continents, each employing their unique growth methods. The data also includes the measurement results obtained with a 50 mm diameter and 30 mm height resonator and with another operating on the WGE modes.

Evidently, the observed distribution of mode splitting is not entirely random. Notably, the mode splitting is higher for modes with m being a multiple of 3 ($m = \text{mult}(3)$), regardless of the crystal's origin, dimensions, or the excited mode family. In the observable frequency range, a maximum occurs for $m = 6$ and then $\delta\nu_m$ decreases with m following a curve parallel to $1/Q_L$, Q_L being the loaded Q-factor. This observation supports the presence of a defect that affects the external shape of the resonator. Higher-order modes being more confined in the dielectric are less impacted by a defect on the resonator surface. For other modes with $m \neq \text{mult}(3)$, the mode splitting is generally not observed or remains of the order of the mode bandwidth. Fig. 5 shows the resonator transmission coefficient $|S_{21}|$ for the two modes $WGH_{9,0,0}$ and $WGH_{10,0,0}$ measured at 6 K. The mode splitting $\delta\nu_9 \approx 30$ kHz is clearly resolved, whereas for $m = 10$ the twin modes can be hardly distinguished.
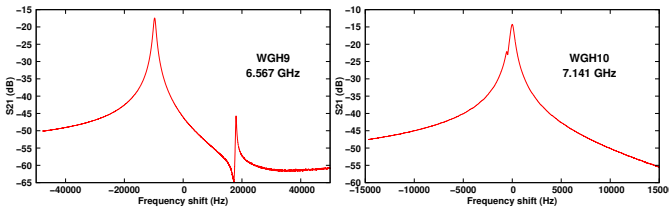
Fig. 5. $|S_{21}|$: *magnitude of the transmission coefficient for the WGH$_{9,0,0}$ and WGH$_{10,0,0}$ modes at 6 K.*

IV. DEDUCTIVE SIMPLIFIED MODEL

It is improbable that identical defects exist on all these resonators with vastly different origins, unless these defects are linked to an intrinsic property of the sapphire crystal. Lu et al. demonstrated for a photonic WG modes micro-cavity that an intentionally modulating the resonator diameter induces controlled mode splitting for a selected azimuthal mode number [31]. The observation that modes with $m = \text{mult}(3)$ exhibit the largest observed mode splitting suggests the presence of a periodic cylindrical defect that would primarily interact with this class of modes. In this section we apply the first order perturbation method to determine a resonator outer shape consistent with the experimental observation reported in Fig. 4.

Let's consider the sapphire resonator with a small geometrical defect placed in the center of a copper cavity delimiting the volume V (see Fig.6).
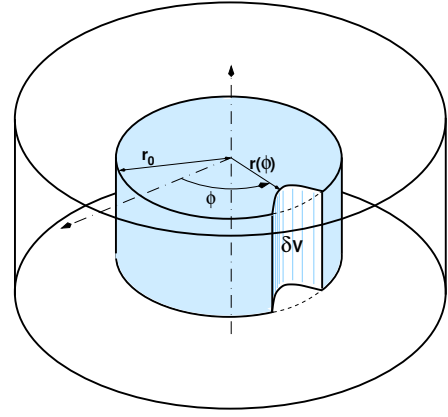
Fig. 6. *Whispering Gallery Mode Sapphire resonator with a small geometrical defect, inserted in the center of the copper cavity. The nominal sapphire resonator radius is r_0. For the ULISS-2G resonator $r_0 = 27$ mm.*

For the unperturbed resonator, the Maxwell's equations are solved using a custom software based on Mode Matching Method [30]. Frequency, Q-factor and the electromagnetic field components for an arbitrary WG mode are calculated knowing the resonator geometry and the material properties. The permittivity tensor describing the material dielectric properties will be denoted $[\epsilon]$. In the empty volume surrounding the sapphire piece, it reduces to the identity matrix $[\epsilon] = [1]$. Inside the sapphire resonator, we have:

$$[\epsilon] = [\epsilon_S] = \begin{bmatrix} \epsilon_t & 0 & 0 \\ 0 & \epsilon_t & 0 \\ 0 & 0 & \epsilon_z \end{bmatrix} \tag{4}$$

with $\epsilon_t \approx 9.27$ and $\epsilon_z \approx 11.37$ at liquid helium temperature [32]

The resonance frequency shift resulting from the geometrical defect can be assessed using the perturbation method [33], [34].

$$\frac{\Delta\nu}{\nu} = \frac{\Delta W_m - \Delta W_e}{W_m + W_e} \tag{5}$$

where ΔW_m and ΔW_e are the changes in the stored magnetic energy and electric energy, respectively, after the shape perturbation, and $W_m + W_e$ is the total stored energy in the cavity. As there is no magnetic material in the cavity $\Delta W_m = 0$. The first order perturbation method assumes that the defect does not modify the electromagnetic field components and thus:

$$\frac{\Delta\nu}{\nu} = \epsilon_0 \frac{\iiint_{\delta V} \mathbf{E} ([\epsilon_S] - 1) \mathbf{E}^* \, \mathrm{d}v}{\iiint_V (\mu_0 \mathbf{H}^2 + \epsilon_0 \mathbf{E}[\epsilon]\mathbf{E}^*) \, \mathrm{d}v} \tag{6}$$

where $\mathbf{E}$ and $\mathbf{H}$ are the electric and magnetic fields of the unperturbed resonator, ϵ_0 and μ_0 are the vacuum permittivity and permeability respectively. δV is the volume affected by the geometrical defect. $\delta V > 0$ corresponds to a dielectric removal.

Expression (6) can be simplified by considering that for a WGH mode, the electric field is principally axial: $\mathbf{E} \approx \mathrm{E}_z(\mathrm{r}, \phi, \mathrm{z})\mathbf{z}$. Moreover, as the deformation is small compared to the sapphire dimensions, $J_m(kr)$ can be considered as a

constant over δV. Taking these approximations in account, it is shown in the Appendix that for a given azimuthal number m, the twin modes will be differently shifted and $\delta \nu_m$ is proportional to:

$$I_m = \int_0^{2\pi} \left(\cos(2m\phi) \int_{r(\phi)}^{r_0} r\, dr \right) d\phi \tag{7}$$

Let us consider a small modulation of the resonator radius such as: $r(\phi) = r_0 + \Delta r \cos(p\phi)$, with p being an integer and $\Delta r \ll r_0$. I_m becomes:

$$I_m = 2r_0 \Delta r \int_0^{2\pi} \cos(2m\phi)\cos(p\phi)\,d\phi \tag{8}$$

I_m takes a non null value only if $p = 2m$. As a first consequence, p should be an even integer to induce mode-splitting. Thus the radius modulation only affects the mode with $m = p/2$, leaving the other WGH modes unperturbed. To obtain a distribution like those in Fig. 4, the radius modulation should be less *smooth*. In other words, $r(\phi)$ should contain harmonics of the fundamental modulation frequency:

$$r(\phi) = r_0 + \Delta r \sum_{j \geq 1} a_j \cos(j \times p\phi) \tag{9}$$

In that condition, I_m becomes the weighted sum of terms proportional to the Fourier coefficients a_j. The jth term takes a non null value for a specific azimuthal number:

$$m_j = j\frac{p}{2} \tag{10}$$

Thus, for a given even integer p, the azimuthal numbers for which a mode splitting appears follow an arithmetic progression with a reason Δm:

$$\Delta m = m_j - m_{j-1} = \frac{p}{2} \tag{11}$$

In our case, we have $m = \text{mult}(3)$, thus $\Delta m = 3$ and:

$$p = 6 \tag{12}$$

From this simple observation, we deduce that the geometric defect must have a periodicity of $\pi/3$ in the azimuthal direction to induce a mode-splitting distribution compatible with the experimental observations.

The shape of the resonator is not yet known. We have now to determine the coefficients of the dependence of the $r(\phi)$. The non null terms in I_m is proportional to the Fourier coefficients a_j such as $j = m/3$. The measured $\delta\nu_m/\nu_m$ gives thus an estimation of the relative value of the Fourier coefficients a_j.

As mentioned earlier, mode splitting for $m = 3$ cannot be determined experimentally. Indeed, the $\text{WGH}_{3,0,0}$ is hardly observable in the standard conditions of the experiment. However, we have, in one case, pushed the resolution of the VNA using high power and averaging and observed a bandwidth of approximately 200 kHz for the $\text{WGH}_{3,0,0}$ mode. Due to the poor signal-to-noise ratio, no mode splitting could be highlighted. We then assume that for the $\text{WGH}_{3,0,0}$

mode, a mode-splitting of the order of magnitude of the line half-bandwidth, i.e., $\delta\nu_3/\nu_3 \sim 3 \times 10^{-5}$, which represents roughly the limit below which the mode splitting cannot be observed. For the other m values, we take the average of the collected data. Setting $a_1 = 1$, we get for the Fourier coefficients up to $j = 6$:

TABLE I
FOURIER COEFFICIENTS OF THE EXPECTED RADIUS DEFORMATION $r(\phi)$

j	m	$\delta\nu/\nu_m$	Fourier Coef.
1	3	(3.0×10^{-5})	$a_1 = 1.000$
2	6	1.0×10^{-5}	$a_2 = 0.333$
3	9	4.5×10^{-6}	$a_3 = 0.150$
4	12	2.0×10^{-6}	$a_4 = 0.067$
5	15	1.0×10^{-6}	$a_5 = 0.034$
6	18	5.0×10^{-7}	$a_6 = 0.017$

The amplitude of the defect Δr remains the only free parameter. Using the perturbational technique based on Eq. (6), we calculated the mode splitting for m ranging from 3 to 24 and various radial deviations Δr. In this analysis, we do not rely on previous approximations; instead, we take into account all electromagnetic fields components, their variation with respect to the coordinates in the entire volume V, and the anisotropy of the dielectric medium. In Fig. 4 the red points represent $\delta\nu_m/\nu_m$ calculated with $\Delta r = 1.3$ μm, which provides the best fit with the experimental observations. The corresponding resonator shape is depicted in Fig. 7 representing $r(\phi) - r_0 + 5$ μm in polar coordinates. Such a homothetic contour plot is classically used by engineers to magnify the representation of circularity defects.
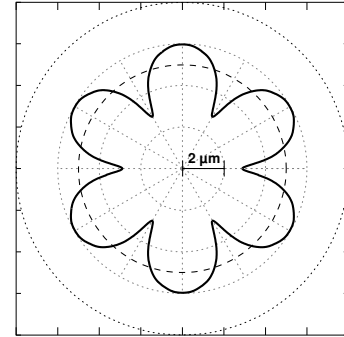
Fig. 7. *Resonator profile derived from the measurement of $\delta\nu_m/\nu_m$ assuming $\Delta r = 1.3$ μm. This homothetic contour plot corresponds to $r(\phi) - r_0 + 5$ μm. The dashed line represents the nominal resonator cylindrical shape with $r_0 = 27$ mm.*

At the first glance, the shape of the resonator deduced from our calculation is astonishing. The calculated resonator profile looks like a flower with six well-defined petals, exhibiting a peak-valley radius deviation of ≈ 3 μm. In the next sections, we will explore how the real profile of the resonator aligns with this calculated shape and provide an explanation for its specific form.

V. ACTUAL RESONATOR PROFILE

The profiles of two sapphire resonators from different manufacturers were measured using a metrological optical

coordinate measuring machine μCMM Bruker Alicona. This instrument allowed the measurement of the resonator contour in its equatorial plane with a resolution of 0.1 μm. Fig. 8 displays the two measured profiles compared to the modelled one (see Fig. 7).
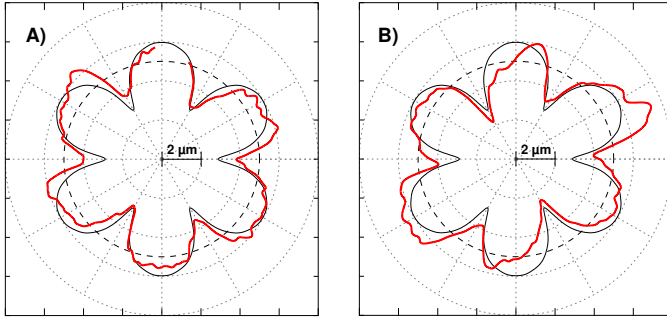
Fig. 8. *Red plain line: Profile of two sapphire resonators measured with a resolution of 0.1 μm. Black plain line: Profile deduced from frequency measurements. Dashed black line: Resonator nominal diameter.*

It is remarkable that the calculated profile faithfully mirrors the actual resonator contour. This comparison fully validates the calculation presented in the previous section. The radius of the two resonators exhibits a modulation with a periodicity of $\pi/3$, and the peak-valley radius deviation is approximately 3 μm, and this same defect is consistently observed in all resonators, regardless of their origin. Consequently, it is reasonable to attribute this defect to an intrinsic property of the sapphire crystal polishing.

VI. CONTOUR DEFECTS AND SAPPHIRE CRYSTAL POLISHING

In the following, a discussion on the intriguing contour of the sapphire resonator is presented from a manufacturing and material perspective. All c-oriented sapphire cylinder were prepared by chemical mechanical polishing (CMP) composed of particles and chemical agent with rotation polishing machine (whose exact production conditions may change from one manufacturer to another). However, the contour presents systematically large curved surfaces and concave engraving defects as shown in Fig. 8 that are schematically redrawn in Fig. 9.

The symmetry of order 6 indicates that one of the prismatic planes a $(11\bar{2}0)$ or m $(10\bar{1}0)$ planes (the first two densest planes perpendicular to the c-plane (1000)) is favoured over to the other. This outcome directly illustrates Neumann's principle, emphasizing the fundamental connection between crystal structures and symmetries, as detailed in Robert Newnham's book [35].

Furthermore, looking carefully at Fig. 8, the curved surfaces show a stepped shape indicating that it corresponds to a crystallographic plane which tends to maintain its flat surface (low surface energy). Rather than following the curvature imposed by the polishing machine, the sapphire piece will keep flat surfaces corresponding to this crystallographic plane. We will then have a succession of parallel steps that will approximate the desired cylindrical surface. This plane

has the slower CMP etching rate (noted V_{slow}) than any other prismatic plane of sapphire. As for the second family of prismatic plane, located at $\pi/6$ to the first one, it presents a concave engraving. This family plane has the fastest polishing rate (noted V_{fast}). The engraving phenomena can be explained by the Rehbinder effect [36]. The polishing chemical agent with the highest surface energy tends to accumulate the polishing particles to this face under the polishing pressure. The particles create microcracks after microcracks penetrating the crystal [37]. Fig. 9 schematizes the polar diagram of the crystal shape with two CMP etching rates. At this level of discussion, the determination of faster and slower CMP etching rate surfaces among the a- or m-planes has not been determined by diffraction X-rays in this study. [38]
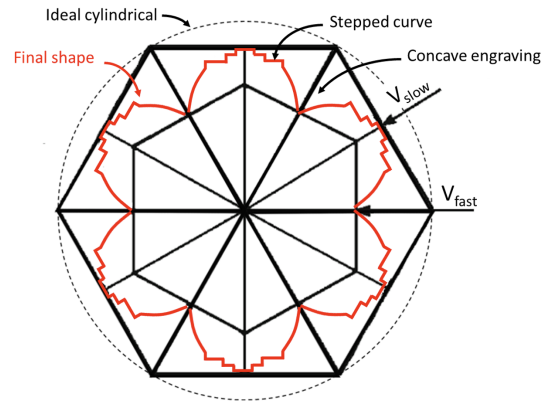
Fig. 9. *Polar diagram representing the crystallographic planes (black lines), the etching rates and the expected final shape (red lines) (figure adapted from [37]).*

The literature presents several conflicting results on the CMP polishing rate of a- and m-planes [39], [40], as well as crystal morphology, surface energy, chemical dissolution and tribological/mechanical tests. Additionally, CMP polishing rate may likely change behavior due to surface atomic relaxation, crystal impurities, surfactant composition, water, wear rotation speed, or temperature [37]. Meanwhile, the surface energy is generally correlated to the friction but also to the hardness and etching rate [37]. In fact, the CMP polishing rates of the two prismatic planes may be very close. This result can be attributed to the close tensorial properties of the a and m planes, particularly up to fourth-order properties. Distinguishing between the two surfaces, as suggested by Le Blois and Tellier's work on crystal etching [41], requires consideration of high-order tensorial properties of the surface. One can note that the final contour gives a very low crystal roughness of 3 μm for a crystal diameter of 54 mm which may depend on the polishing time. The relative tolerance of 6×10^{-5} in micro-machining is in the state of the art for anisotropic crystal. Finally, another argument in favor of the Rehbinder effect can be seen in Fig. 8. Almost all stepped shape and engraving defects have an asymmetrical shape tilted in the same direction, which is likely the direction of polishing rotation.

VII. Summary

In this paper we have solved the problem of the origin of the mode splitting effect in the cylindrical sapphire whispering gallery mode resonator. The same mode splitting repartition as a function of the azimuthal mode order is effectively observed in any sapphire resonator whatever their origin. Consequently, we have deduced that mode splitting results from a 6-fold modulation in the radius of the resonator contour, a consequence of the resonator polishing step. This study serves as an illustration of Neumann's principle, emphasizing that, despite meticulous attention during the manufacturing of crystalline cylinders, the inherent symmetry of crystals takes precedence at the finest scales of micro-fabrication. In the case of sapphire, the properties of the prismatic plane remain remarkably consistent up to the 4th tensorial order, allowing for the production of quasi-cylinders. Nevertheless, as proposed by Tellier and her colleagues, the variation in surface slowness is influenced by higher-order tensor terms. The observed mode splittings enable to calculate an approximate resonator profile, which is confirmed with high resolution resonator contour measurements.

Finally, our results, which seem to demonstrate that we can calculate the shape of a body from the spectrum of its resonances, do not, of course, question the work of mathematicians. This is a very specific case, where we determine only the irregularities of a known form, here a cylinder, from a peculiarity of the spectrum of its resonances, and theorems that prove the isospectrality of distinct geometries certainly do not apply. However, the similarity between the calculated contour and the actual profile is surprising and, in our view, deserves to be highlighted.

VIII. Acknowledgment

Appendix I:
Derivation of Expression (7)

The general equation (6) can be simplified for WGH modes by assuming: i) the electric field is axial, and ii) all the energy is stored within the dielectric. We thus neglect the electromagnetic fields components in the empty volume surrounding the sapphire cylinder. Moreover, at resonance, the stored magnetic and electric energies are equals. Expression (6) can be rewritten as:

$$\frac{\Delta \nu}{\nu} = \frac{(\epsilon_z - 1)}{2\epsilon_z} \frac{\iiint_{\delta V} E_z^2(r, \phi, z) dv}{\iiint_{V_S} E_z^2(r, \phi, z) dv} \quad (13)$$

where V_S is the volume of the sapphire cylinder.

For a given azimuthal number m, the first solution of the Helmholtz equation corresponds to an electric field varying as $\cos(m\phi)$ along the azimuthal direction:

$$E_z(r, \phi, z) = E_m J_m(kr) \cos(\beta z) \cos(m\phi) \quad (14)$$

Replacing E_z in Eq. (13) by this expression and assuming $J_m(kr)$ constant over δV, the frequency shift is:

$$\left. \frac{\Delta \nu_m}{\nu_m} \right|_c = K_m \int_0^{2\pi} \left(\cos^2(m\phi) \int_{r(\phi)}^{r_0} r dr \right) d\phi \quad (15)$$

with

$$K_m = \frac{(\epsilon_z - 1)}{2\pi\epsilon_z} \frac{J_m^2(kr_0)}{\int_0^{r_0} r J_m^2(kr) dr} \quad (16)$$

Strictly speaking K_m is a function of the azimuthal order. However, its variations are small as shown on Fig 10 where is drawn K_m/K_{15}.
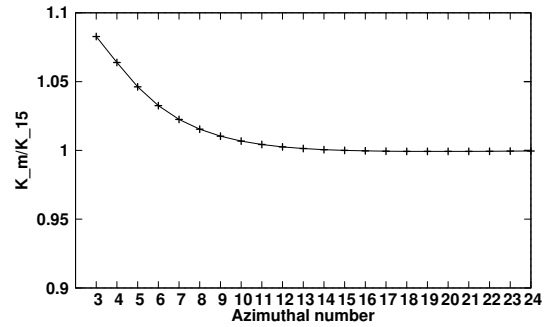
Fig. 10. K_m as a function of the azimuthal number m.

For $m \geq 3$, K_m does not deviate by more than 10% from its asymptotic value, and we will neglect this variation considering K_m as a constant independent of the value of m:

$$K_m = K \qquad \forall \, m \quad (17)$$

The second solution of the Helmholtz equation varies as $\sin(m\phi)$ and likewise:

$$\left. \frac{\Delta \nu_m}{\nu_m} \right|_s = K \int_0^{2\pi} \left(\sin^2(m\phi) \int_{r(\phi)}^{r_0} r dr \right) d\phi \quad (18)$$

Eventually the mode splitting is given by:

$$\frac{\delta \nu_m}{\nu_m} = \left. \frac{\Delta \nu_m}{\nu_m} \right|_c - \left. \frac{\Delta \nu_m}{\nu_m} \right|_s \quad (19)$$

Dropping the constant K, the mode splitting is found proportional to I_m given by Eq. (7).

References

[1] C. Fluhr, B. Dubois, S. Grop, J. Paris, G. Le Tetû, and V. Giordano, "A low power cryocooled autonomous ultra-stable oscillator," *Cryogenics*, vol. 80, pp. 164–173, 2016.

[2] X. Zhu, H. Chen, K. Huang, and L. Gao, "Analytical analysis method of whispering gallery mode of sapphire dielectric resonators and the optimization of the Q value in liquid helium temperature," in *Proc. 2018 China Satellite Navigation Conf. (CSNC): Volume I*, pp. 623–632, Springer, 2018.

[3] C. R. Locke, E. N. Ivanov, J. G. Hartnett, P. L. Stanwix, and M. E. Tobar, "Invited article: Design techniques and noise properties of ultrastable cryogenically cooled sapphire-dielectric resonator oscillators,"*Rev. of Sci. Instrum.*, vol. 79, no. 5, 2008.

[4] S. Vitusevich, K. Schieber, I. Ghosh, N. Klein, and M. Spinnler, "Design and characterization of an all-cryogenic low-phase-noise sapphire K-band oscillator for satellite communication," *IEEE Trans. on Microw. Theor. Techn.*, vol. 51, pp. 163–169, Jan. 2003.

[5] J. Krupka, K. Derzakowski, A. Abramowicz, M. Tobar, J. Hartnett, and R. Geyer, "Use of whispering-gallery modes for complex permittivity determinations of ultra-low-loss dielectric materials," *IEEE Trans. on Microw. Theor. Techn.*, vol. 47, pp. 752–759, 1999.

[6] N. Cherpak, A. Barannik, Y. Filipov, Y. Prokopenko, and S. Vitusevich, "Accurate microwave technique of surface resistance measurement of large-area hts films using sapphire quasi-optical resonator," *IEEE Trans. on Appl. Supercond.*, vol. 13, no. 2, pp. 3570–3573, 2003.

[7] X. H. Jiao, P. Guillon, L. A. Bermudez, and P. Auxemery, "Whispering-gallery modes of dielectric structures: Applications to millimeter-wave bandstop filters," *IEEE Trans. on Microw. Theor.Techn.*, vol. 35, no. 12, pp. 1169–1175, 1987.

[8] D. Cros and P. Guillon, "Whispering gallery dielectric resonator for W-band devices," *IEEE Trans. on Microw. Theor. Techn.*, vol. 38, pp. 1667–1674, Nov. 1990.

[9] A. B. Matsko and V. S. Ilchenko, "Optical resonators with whispering-gallery modes-part i: basics," *IEEE J. of Sel. Top. Quant. Electron.*, vol. 12, no. 1, pp. 3–14, 2006.

[10] V. S. Ilchenko and A. B. Matsko, "Optical resonators with whispering-gallery modes-part ii: applications," *IEEE J. of Sel. Top. Quant. Electron*, vol. 12, no. 1, pp. 15–32, 2006.

[11] P.-Y. Bourgeois and V. Giordano, "Simple model for the mode splitting effect in whispering gallery mode resonators," *IEEE Trans. on Microw. Theor. Techn.*, vol. 53, pp. 3185–3190, Oct. 2005.

[12] Q. Li, A. A. Eftekhar, Z. Xia, and A. Adibi, "Unified approach to mode splitting and scattering loss in high-Q whispering-gallery-mode microresonators," *Phys. Rev. A*, vol. 88, no. 3, p. 033816, 2013.

[13] Y. Filipov, S. Kharkovsky, and A. Kirichenko, "Whispering-gallery modes of nonuniform dielectric resonators," *Microw. and Opt. Techn. Lett.*, vol. 10, no. 2, pp. 124–129, 1995.

[14] X. Yi, Y.-F. Xiao, Y.-C. Liu, B.-B. Li, Y.-L. Chen, Y. Li, and Q. Gong, "Multiple-rayleigh-scatterer-induced mode splitting in a high-Q whispering-gallery-mode microresonator," *Phys. Rev. A*, vol. 83, no. 2, p. 023803, 2011.

[15] D. G. Santiago, G. J. Dick, and A. Prata, "Mode control of cryogenic whispering-gallery mode sapphire dielectric-ring resonator," *IEEE Trans. on Microw. Theor. Techn.*, vol. 42, pp. 52–55, Jan. 1994.

[16] O. Di Monaco, Y. Kersalé, and V. Giordano, "Resonance degeneration and spurious mode suppression in a cryogenic whispering gallery mode sapphire resonator," *IEEE Microw. and Guid. Wave Lett.*, vol. 10, pp. 368–370, Sept. 2000.

[17] E. N. Ivanov and M. E. Tobar, "Noise suppression with cryogenic resonators," *IEEE Microw. and Wireless Compon. Lett.*, vol. 31, no. 4, pp. 405–408, 2021.

[18] T. J. Kippenberg, "Particle sizing by mode splitting," *Nature Photon.*, vol. 4, no. 1, pp. 9–10, 2010.

[19] X. Jiang, A. J. Qavi, S. H. Huang, and L. Yang, "Whispering-gallery sensors," *Matter*, vol. 3, no. 2, pp. 371–392, 2020.

[20] M. Kac, "Can one hear the shape of a drum?," *The American Math. Monthly*, vol. 73, no. 4P2, pp. 1–23, 1966.

[21] C. Gordon, D. L. Webb, and S. Wolpert, "One cannot hear the shape of a drum," *Bulletin of the American Math. Soc.*, vol. 27, no. 1, pp. 134–138, 1992.

[22] S. Sridhar and A. Kudrolli, "Experiments on not "hearing the shape"of drums," *Phys. Rev. Lett.*, vol. 72, no. 14, p. 2175, 1994.

[23] V. Branginsky, V.S.Ilchenko, and K. Bagdassarov, "Experimental observation of fundamental microwave absorption in high quality dielectric crystal," *Phys. Lett. A*, vol. 120, pp. 300–305, Mar. 1987.

[24] C. Fluhr, B. Dubois, G. Le Tetu, V. Soumann, J. Paris, E. Rubiola, and V. Giordano, "Reliability and reproducibility of the cryogenic sapphire oscillator technology," *IEEE Trans. on Instrum. Meas.*, vol. 72, pp. 1–8, June 05 2023.

[25] C. Fluhr, B. Dubois, C. E. Calosso, F. Vernotte, E. Rubiola, and V. Giordano, "A cryogenic sapphire resonator oscillator with 10^{-16} mid-term fractional frequency stability," *Appl. Phys. Lett.*, vol. 123, p. 044107, 07 2023.

[26] https://www.femto-engineering.fr/en/realisation/uliss-cryogenic-sapphire-oscillator/.

[27] V. Giordano, C. Fluhr, S. Grop, and B. Dubois, "Tests of sapphire crystals manufactured with different growth processes for ultra-stable microwave oscillators," *IEEE Trans. on Microw. Theor. Techn.*, vol. 64, pp. 78–85, Jan. 2016.

[28] S. Grop, P. Y. Bourgeois, N. Bazin, Y. Kersalé, E. Rubiola, C. Langham, M. Oxborrow, D. Clapton, S. Walker, J. De Vicente, and V. Giordano, "ELISA: A cryocooled 10 GHz oscillator with 10^{-15} frequency stability," *Rev. of Sci. Instrum.*, vol. 81, no. 2, p. 025102, 2010.

[29] C. G. Montgomery, *Technique of microwave measurements*. Radiation Laboratory series, no. 11., McGraw-Hill Book Co., 1947.

[30] E. Ivanov, D. Blair, and V. Kalinichev, "Approximate approach to the design of shielded dielectric disk resonators with whispering gallery modes," *IEEE Trans. on Microw. Theor. Techn.*, vol. 41, pp. 632–638, Apr. 1993.

[31] X. Lu, A. Rao, G. Moille, D. A. Westly, and K. Srinivasan, "Universal frequency engineering tool for microcavity nonlinear optics: multiple selective mode splitting of whispering-gallery resonances," *Photon. Res.*, vol. 8, no. 11, pp. 1676–1686, 2020.

[32] J. Krupka, K. Derzakowski, M. Tobar, J. Hartnett, and R. Geyer, "Complex permittivity of some ultralow loss dielectric crystals at cryogenic temperatures," *Meas. Sci. Technol.*, vol. 10, pp. 387–392, 1999.

[33] E. Argence and T. Kahan, *Théorie des guides et cavités électromagnétiques*. Dunod, 1964.

[34] D. M. Pozar, *Microwave engineering*. John Wiley & Sons, 2011.

[35] R. E. Newnham, *Properties of materials: anisotropy, symmetry, structure*. Oxford University Press, 2005.

[36] Y. J. Lee and H. Wang, "Current understanding of surface effects in microcutting," *Mater. & Des.*, vol. 192, p. 108688, 2020.

[37] E. R. Dobrovinskaya, L. A. Lytvynov, and V. Pishchik, *Sapphire: material, manufacturing, applications*. Springer Science & Business Media, 2009.

[38] M. B. Smith, F. Schmid, C. P. Khattak, K. A. Schmid, D. Golini, J. C. Lambropoulos, M. A. Atwood, Y. Zhou, and P. D. Funkenbusch, "Sapphire fabrication for precision optics," in *Adv. Mater. for Opt. Precis. Struct.*, vol. 2857, pp. 99–112, SPIE, 1996.

[39] H. Zhu, L. A. Tessaroto, R. Sabia, V. A. Greenhut, M. Smith, and D. E. Niesz, "Chemical mechanical polishing (CMP) anisotropy in sapphire," *Appl. Surf. Sci.*, vol. 236, no. 1-4, pp. 120–130, 2004.

[40] L. Wang, Z. Hu, Y. Chen, Y. Yu, and X. Xu, "Material removal mechanism of sapphire substrates with four crystal orientations by double-sided planetary grinding," *Ceram. Int.*, vol. 46, no. 6, pp. 7813–7822, 2020.

[41] T. Leblois and C. Tellier, "Determination of the dissolution slowness surface by study of etched shapes i. morphology of the dissolution slowness surface and theoretical etched shapes," *Journal de Physique III*, vol. 2, no. 7, pp. 1259–1286, 1992.

IX. Biography

Vincent Giordano was born in Besançon, France, on February 20, 1962. He received a Engineer degree in mechanics (five years degree) in mechanics in 1984 from the Ecole Supérieure de Mécanique et des Micro-techniques, Besançon, France, and his PhD in 1987 in Physical Sciences from the Paris XI University, Orsay, France. During 1984-1993 he was researcher of the permanent staff of the Laboratoire de l'Horloge Atomique, Orsay, France, where he worked on a laser diode optically pumped cesium beam frequency standard. In 1993, he joined the Laboratoire de Physique et de Métrologie des Oscillateurs (LPMO), Besançon, France. FEMTO-ST was founded in January 2004 from the merger of 5 different laboratories active in different fields of engineering science: mechanics, optics and telecommunications, electronics, time-frequency, energetics and fluidics. The Department Time & Frequency was created in 2006 grouping all the activities related to Time and frequency metrology and to micro-acoustics components and systems. His current research interests include ultra high stability microwave oscillators based on sapphire resonators, microwave and optical atomic clocks and Time & Frequency metrology.

Samuel Margueron received his master's degree in 2000 at the Magistère de Physique Fondamentale d'Orsay. He obtained his Ph.D. in 2003 at ONERA in the non-destructive testing of turbine blades for jet engines at high temperatures using optical and ultrasonic methods. He spent 2 years as a post-doc at UC Santa Barbara, focusing on the micromechanics of alumina oxide. Since 2008, he has been working on lead-free piezoelectric materials, specifically LiNbO3, and thin film growth. He holds 1 patent, has published 52 papers, and has given more than 20 invited talks. In 2021, Samuel Margueron established the piezoMEMS group ($\sim$ 20 people) at the FEMTO-ST Institute, focusing on electro-active materials, electronic conditioning, and simulations. S.M. is a member of the Board of the French Society of Microtechnology and Chronometry SFMC.